Graphical Abstract

Structure and electronic states of strongly interacting metal-organic interfaces: CuPc on Cu(100) and Cu(110)

H. Okuyama, S. Kuwayama, Y. Nakazawa, S. Hatta, T. Aruga

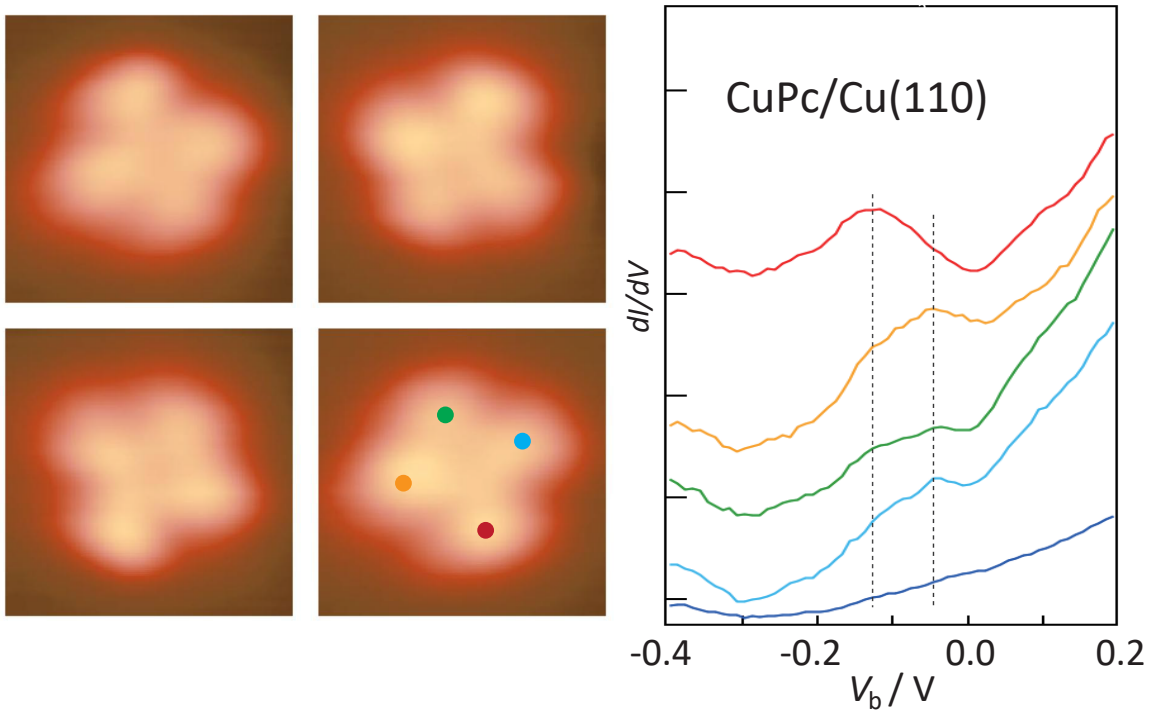

Highlights

Structure and electronic states of strongly interacting metal-organic interfaces: CuPc on Cu(100) and Cu(110)

H. Okuyama, S. Kuwayama, Y. Nakazawa, S. Hatta, T. Aruga

- The CuPc molecules on Cu(100) and Cu(110) belong to the C_4 and C_1 point groups, respectively.
- The CuPc adsorbs on Cu(100) with the center ion located at the hollow site.
- The LUMO levels of CuPc on Cu surfaces are determined.

Structure and electronic states of strongly interacting metal-organic interfaces: CuPc on Cu(100) and Cu(110)

H. Okuyama[a], S. Kuwayama[a], Y. Nakazawa[a], S. Hatta[a], T. Aruga[a]

[a] *Department of Chemistry, Graduate School of Science, Kyoto University, Kyoto, 606-8502, Japan*

Abstract

The structure and electronic states of copper phthalocyanine (CuPc) on Cu(100) and Cu(110) were studied mainly using scanning tunneling microscopy/spectroscopy (STM/STS). We observed that the molecule adsorbs flat on Cu(100), and the lowest unoccupied molecular orbital (LUMO, e_g) is shifted down to the Fermi level, which indicates a partially filled state. The inherent fourfold symmetry of the molecule remains intact upon adsorption, and thus, the degeneracy of LUMO is maintained on the surface. Conversely, the molecule adsorbs in a low-symmetry configuration on Cu(110) and preferentially forms a dimer. Thus, the degeneracy of LUMO is lifted, and the split LUMO is shifted below the Fermi level. We propose that the hybridization with surface d band plays an important role in the energy level alignment and its structure dependence for CuPc on Cu surfaces.

Keywords: Scanning tunneling microscope, Cu phthalocyanine
PACS: 0000, 1111

1. Introduction

Organic thin films grown on metal electrodes have received considerable attention for their application in optelectronic devices such as organic light emitting diodes and solar cells [1]. In addition, electrical measurements of single molecular junctions have been conducted extensively, aiming at the use of individual molecules as a component of electronic devices [2]. The performance of these devices depends mainly on the electronic properties of the molecules in contact with metal electrodes; these properties determine the electron transport efficiency across the interface [3, 4, 5, 6]. As the gas-phase

molecules approach the metal surfaces, depending on the nature of interaction and the interface structure geometry, their discrete electronic levels are perturbed [7, 8, 9, 10]. Therefore, considerable effort has been devoted to understanding the electronic states of organic molecules interacting with various metal surfaces [11, 12, 13, 14, 15, 16, 17, 18, 19]. The energy level alignment of the lowest unoccupied molecular orbital (LUMO) with respect to the Fermi level ($E_{\rm F}$) is particularly important because it is associated with the electron injection barrier from the surface to the molecule. When a closed-shell molecule is put close to metal surface, the spilling-out electron cloud would be pushed back to the surface due to Pauli repulsion, modifying the metal work function and causing the downshift of LUMO level [11, 20]. The downshift is also caused by the variation of the effective potential as the molecule is moved toward the surface, including image-potential (screening) effect [10, 16, 21]. Furthermore, the hybridization with metal states may perturb the LUMO level [7, 8, 9]: In the weak chemisorption limit, it is broadened with additional level shift to form a virtual state within metal bands. The strong hybridization causes the splitting outside of the metal bands, corresponding to the bonding and antibonding orbital formation.

In general, the interaction of organic molecules with Au(111) is relatively weak compared to that with Cu(111) [12, 13, 15, 22]. This is understood in analogy to the argument for the nobleness of gold [23]. When a molecule adsorbs on the surface, the interaction of the molecular orbital with filled d bands of metal surface requires the energy cost for orthogonalization due to pauli repulsion, which is larger for more extended 5d orbital (Au) than 3d orbital (Cu). As a result, the adsorption of organic molecule results in larger adsorption height and smaller adsorption energy on the Au surface. As the adsorption height is smaller, the LUMO shifts to lower energy. For example, the LUMO of 3,4,9,10-perylene-tetracarboxylic acid dianhydride (PTCDA) is located at 0.8 eV below $E_{\rm F}$ on Cu(111) [12], whereas it is located at 0.73 and 1.08 eV above $E_{\rm F}$ for the molecules in the different domains on Au(111) [22]. In the former case, LUMO is hybridized with metal states and significant electron transfer from the metal to the molecule takes place. The interaction with Ag(111) is intermediate, where the former LUMO is located at $\sim$0.3 eV below $E_{\rm F}$ and is partially occupied [24, 25].

Furthermore, the LUMO energy level depends sensitively on the surface structure. Willenbockel et al. studied the electronic states of PTCDA molecule on three low-index Ag surfaces, and found that the energy level of LUMO correlates well with the work function of bare metal surfaces (ϕ_0).

The LUMO is the most stabilized at the open (110) surface with the lowest work function: it is located at -0.7 eV for Ag(110) (ϕ_0=4.05 eV), -0.5 eV for Ag(100) (ϕ_0=4.23 eV) and -0.2 eV for Ag(111) (ϕ_0=4.40 eV). Thus, the energy level of LUMO at Ag surfaces was proposed to be determined mainly by the work function of bare surfaces.

Conversely, the energy level alignment and its dependence on the surface structure is not well understood for Cu surfaces, despite the importance of its application in electrodes. Although there exist extensive studies regarding organic molecules on Cu(111) [26, 27, 28, 29, 30, 31], less attention has been given to the local geometry and electronic states for those on Cu(100) [28, 32, 33, 34] and Cu(110) [35, 36]. Information regarding the electronic states for these surfaces helps in the systematical understanding of the interaction between organic molecules and Cu surfaces. In this study, we analyzed the LUMO of copper phthalocyanine (CuPc) molecule on Cu(100) and Cu(110) to understand the dependence of the energy level alignment on the surface structure. The local geometry and electronic states were studied mainly using scanning tunneling microscopy (STM). It is a unique tool that enables simultaneous characterization of the structure and electronic states at a level of individual molecules, and has been employed to study the electronic states of adsorbed CuPc molecules situated in well-defined local environments [26, 27, 30, 37, 38, 39, 40]. In particular, the LUMO is located at $E_{\rm F}$ (partially occupied) for CuPc on Cu(100), whereas it is located at $\sim$0.1 eV below $E_{\rm F}$ (almost occupied) for that on Cu(110). Combining the result for CuPc on Cu(111) ($\sim$0.5 eV below $E_{\rm F}$) in the literatures [26, 29] with the results of our experiments, we discuss the mechanism of energy level alignment of CuPc on Cu surfaces.

2. Experiments

The STM experiment was conducted at 6 K in an ultrahigh vacuum chamber (USM-1200, Unisoku), using an electrochemically etched W or PtIr tip as the STM probe. Single crystalline Cu(100) and Cu(110) surfaces were cleaned by repeated cycles of argon ion sputtering and annealing. The solid CuPc or ZnPc was sublimated from a crucible heated at 610 K to the surface. The sample was exposed to the vapor at 300 K, and then transferred to the STM at 6 K or 78 K for measurement within 10 min. The scanning tunneling spectra (STS) and its spatial mapping were obtained using the lock-in technique with the modulation voltage of 20 $\rm mV_{rms}$ at 200 Hz. The

tip height was fixed at the set point of the sample voltage V_s = -0.4 V and tunneling current I = 1 nA at the individual positions. The STS spatial mappings were conducted as follows: First, the tip was positioned over one lobe of the CuPc molecule at the set point of V_s=-1.0 V and I = 1 nA; then, the feedback was turned off and the molecule was probed at constant tip height for the STS intensity mappings. At each position, the dI/dV_s and I values were recorded at selected V_s, enabling simultaneous acquisition of dI/dV_s and current images in a single scan. The lateral manipulation of individual CuPc molecules was conducted in the following way: First, the tip was positioned over one CuPc lobe. Then, with the feedback disabled, the tip was moved close to the molecule, until the molecule was lifted up to the tip [41]. Finally, the tip was laterally displaced along the surface to move the molecule. By lifting the molecule with the tip, it is possible to displace even chemisorbed molecules. The probability that the molecule will move as expected on Cu surfaces was low compared to that on Au(110) [39], which may be due to the stronger interaction between the molecule and the Cu surfaces.

The oxygen atoms or nitric oxide (NO) molecules were coadsorbed with CuPc on Cu(100). The surface was exposed to NO gas via a tube doser positioned ∼1 cm from the surface in the STM. The exposure at 78 K results in the dissociation of NO on the surface, and the adsorption of oxygen atoms at the hollow sites (nitrogen atom are desorbed as N_2O) [42]. From their relative position to coadsorbed oxygen atoms, the adsorption site of CuPc was determined. Conversely, the exposure at ∼10 K results in molecular adsorption [42]. The coadsorbed NO molecules were used to prepare a NO-modified tip to image the molecular orbital of CuPc. The NO-modified tip was obtained by scanning the NO-adsorbed surface at V_s = 10 mV and I = 5 nA.

The vibrational state of adsorbed CuPc was characterized by electron energy loss spectroscopy (EELS, LK-5000, LK Technologies, Inc.) in a separate chamber. We used the primary electron energy of 5 eV, incidence angle of 60°, reflection angle of 60° with respect to the surface normal, and typical energy resolution of 3 meV (the full width at half maximum of the elastic peak). Most of the vibration modes observed in this work were confirmed to be excited via dipole scattering mechanism by the angle-dependent measurement of the peak intensities. The EELS measurement was conducted at 300 K.

3. Results

3.1. CuPc on Cu(100)

Figure 1(a) shows a typical STM image of CuPc molecules on Cu(100). Even at higher coverage, the molecules were dispersed and did not form islands, suggesting that the intermolecular interactions is repulsive for CuPc on Cu(100). The molecule lies flat with the axis along the opposing phenyl rings rotated by $\sim \pm 25^\circ$ from the high-symmetry [011] direction; this is in agreement with previous STM studies [28, 32]. The position of CuPc at the surface was determined by the STM image obtained by NO-modified tip [Fig. 1(b)]. The image shows atomic resolution of Cu(100) surface, and thus enables to determine the position of the molecule on the surface. The solid lines represent the lattice of surface Cu atoms, from which it is derived that the molecular center is positioned at a hollow site. Note that the surface Cu atoms appear to be dark in the STM image when probed with a NO-modified tip of p-orbital character, as discussed in the Appendix. The position was also investigated with a normal tip by recording STM images of CuPc coadsorbed with oxygen atoms which are known to be adsorbed at the hollow sites (Fig. S1). From their relative location, the center Cu ion was confirmed to be positioned at a hollow site. Thus, the molecule belongs to the point group of C_4, as shown schematically in Fig. 1(c).

The electronic states of CuPc on Cu(100) were investigated by STS [Fig. 2(a)]. The spectra were recorded at each position shown in the inset. The bottom spectrum was recorded over the clean surface. Other spectra show a peak near E_{F} over the molecule, and the intensity is higher at the molecular center than at the lobes. Figure 2(b) shows the STS intensity mapping of the peak (V_{s}=0.02 V). The current intensity (V_{s}=0.5 V) was recorded simultaneously in Fig. 2(c), which shows the location of the molecule. These data illustrate that the peak intensity is distributed over the molecule with the maximum at the molecular center. In order to identify the origin of the peak, the STS were also conducted for ZnPc which has d^{10} configuration, as compared to d^9 configuration for CuPc (Fig. S2). The STM image of ZnPc on Cu(100) was not distinguishable from that of CuPc, and the STS show the same peak as for CuPc. Therefore, the peak in Fig. 2(a) is assigned to the LUMO distributed across the ligand π orbital, rather than the d orbital originated from the metal center. The LUMO is degenerate (e_g under point group of D_{4h}), and its outline of gas-phase CuPc is depicted in Fig. 2(d).

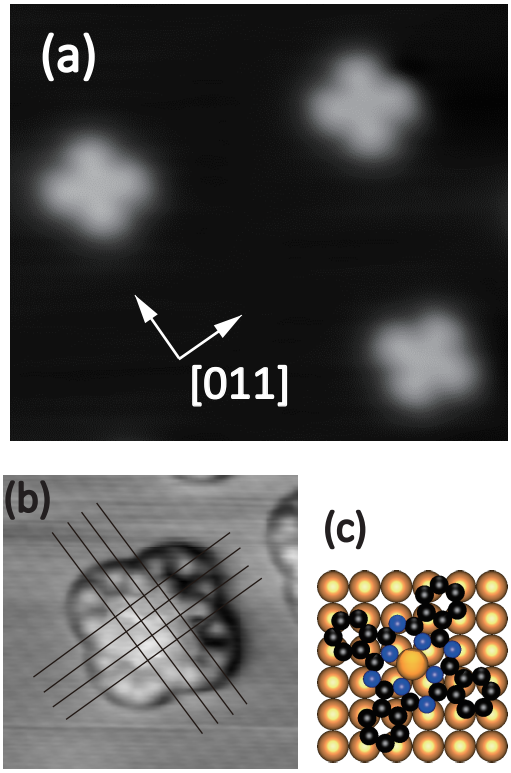

Figure 1: (a) STM images of CuPc molecules on Cu(100) at 6 K obtained at V_s=-0.1 V and I = 1 nA. The image size is 9.0 × 7.9 nm. (b) STM image of a CuPc molecule obtained with a NO-modified tip at V_s=-0.01 V and I = 5 nA. The solid lines represent the lattice of Cu(100). The image size is 3.9 × 3.9 nm. (c) Schematic illustration of a CuPc molecule on Cu(100). The molecule is positioned with the center Cu ion on the hollow site of Cu(100).

The LUMO is shifted down to the E_{F} as a result of the interaction with the surface, and broadened due to the hybridization with metal states.

For the π-conjugated molecules on metal surfaces, the STM imaging performed using a tip with p-orbital character can provide information about the molecular orbital responsible for the conductance [43]. We used a NO-modified tip for imaging the orbital of CuPc on Cu(100) [Fig. 1(b)]. The p-orbital character of the NO tip allows it to couple with the nodal points of the molecular orbitals, and thus, the image reflects lateral gradient of the molecular orbital [44, 45]. Figure 1(b) shows intramolecular structure in the isoindole moiety of the ligand, which is consistent with the lateral gradient of LUMO (See Appendix). This suggests that the dI/dV_{s} peak at E_{F} is ascribed to LUMO and the contribution from the d orbital of the metal center is relatively small.

Notably, the peaks in Fig. 2(a) appear to be asymmetric especially for those recorded over the molecular lobes. This feature is reproducible and does not depend on the tip condition. These peaks are well reproduced by the Fano line shape for conductance, i.e., $dI/dV_{\mathrm{s}} \propto \frac{(q+\epsilon)^2}{1+\epsilon^2}$, where q is the Fano parameter and $\epsilon = \frac{eV_{\mathrm{s}}-\epsilon_0}{\Gamma/2}$, where $-e$ is elementary charge of electron, ϵ_0 the LUMO energy level and Γ the resonance width [46]. The result of the fitting is shown in Fig. S3, considering the LUMO level ϵ_0=0.0 eV and Γ=0.20$\pm$0.01 eV. The asymmetry of the peak is reflected in q, which is 2.3$\pm$0.2 and 2.0$\pm$0.3 for the spectra over the molecular center and over the lobe, respectively. The large q value represents the spectra of symmetric Lorentzian shape, and an asymmetric feature appears as q decreases to 1. Because the discrete molecular state (LUMO) is located at E_{F} and hybridized with the metal continuum states, the electron transport through the molecule shows interference effect between the conductance channels, giving rise to the Fano resonance in the dI/dV conductance spectra [46, 47].

Figure 3 shows EEL spectra of Cu(100) as a function of exposure to CuPc vapor at 300 K. At the initial exposure (up to 3 min), peaks were observed at 21, 53, 70, 77, 90, 134, and 181 meV (indicated by ticks), which were ascribed to vibration modes of CuPc on the surface. After the exposure of 380 min, additional peaks were observed at 43, 98, and 379 meV, along with slight frequency shift of the original peaks. These peaks were ascribed to the molecules, which are free from direct contact with the surface and are more likely to be located in the second layer. For the molecules directly adsorbed on the surface, the active modes are limited by the dipole selection

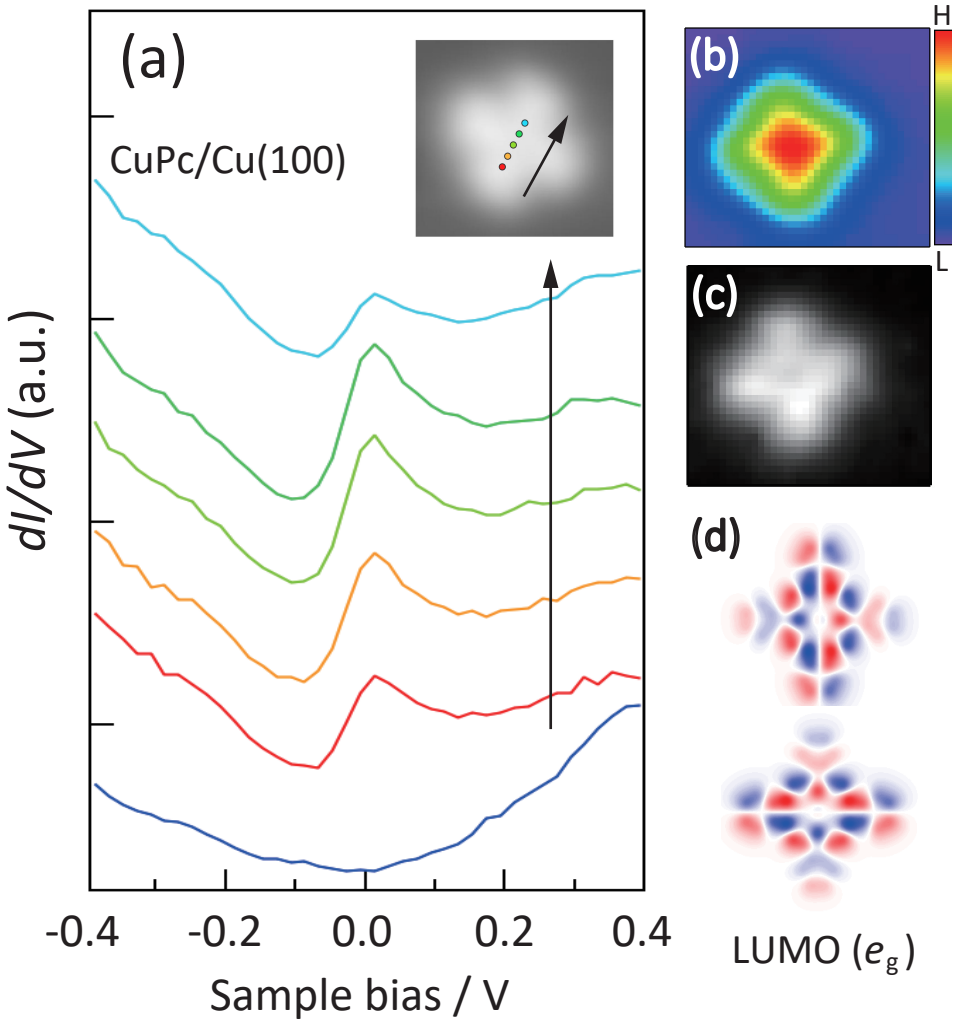

Figure 2: (a) STS of CuPc molecules on Cu(100) at 6 K obtained at each point across the molecule shown in the inset. (b) Spatial map of the STS peak intensity at V_s= 0.02 V obtained in constant-height mode (3.3 × 3.0 nm). (c) Simultaneously recorded current map at V_s= 0.5 V. (d) Outline of the wavefunction $\phi(x, y, z_0)$ for LUMO (e_g) of free CuPc molecule.

rule of EELS, i.e., only the totally symmetric modes are allowed. Out of the infrared or Raman active modes for free CuPc [48, 49, 50], the A_{2u} and A_{1g} modes are totally symmetric when the molecule adsorbs on the surface in the C_4 symmetry. In particular, for planer molecules adsorbed in a flat geometry, the A_{2u} mode exhibits a relatively high intensity because it is polarized along the surface normal. Accordingly, we assign the peaks observed at low exposure (ticks in Fig. 3) mainly to the A_{2u} modes, as shown in Table I. The most intense peak at 90 meV is assigned to the out-of-plane bending (OPB) mode of the C–H bond. The corresponding infrared peak for solid CuPc was observed at 90 meV; the vibration energy of the OPB C–H mode is unaffected by the adsorption on Cu(100). The 53 meV peak is also safely assigned to the OPB mode of benzene ring (54 meV for solid CuPc) [50]. By contrast, the 77 meV peak was not observed either for solid CuPc or CuPc weakly adsorbed on Au(100) [51]. We assigned this new peak to the OPB mode of C-N-C and/or C-C-N, which appears as a result of the molecule–surface interaction. The tiny 70 meV peak is possibly due to the ring breathing and Cu–N stretch mode (A_{1g}) observed at 74 meV for solid CuPc [49]. The 21 meV peak can be assigned to the OPB mode of the Cu–N bond, based on the theoretical prediction [50]. The 134 and 181 meV peaks are assigned to the in-plane bending (IPB) C–H modes. The C–H stretch mode was only observed for the second-layer molecules (inset in Fig. 3). The weak intensities of the IPB and C–H stretch modes are consistent with the case where the molecule is in a flat configuration on the surface.

Table 1: Vibrational energies, symmetry species and approximate description of vibration modes observed for low-coverage CuPc on Cu(100).

Energy (meV)	Symbol	Description
21	A_{2u}	Cu-N OPB
53	A_{2u}	C-C-C OPB
70	A_{1g}	Ring breath, Cu-N stretch
77	A_{2u}	C-N-C, C-C-N OPB
90	A_{2u}	C-H OPB
134	A_{1g}	C-H IPB
181	A_{1g}	C-H IPB

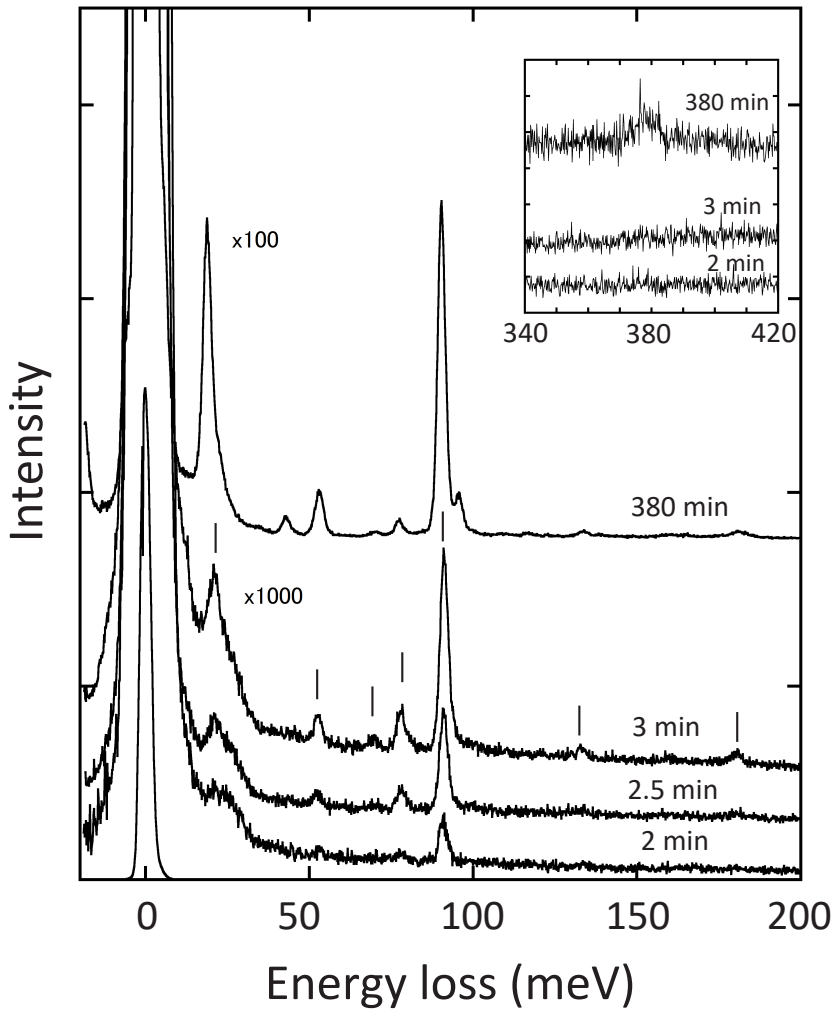

Figure 3: EEL spectra of CuPc on Cu(100) as a function of exposure time. The inset shows the C-H stretch region. At the initial stage of exposure (up to 3 min), the molecule is adsorbed on the surface and the vibration modes derived from the molecule are indicated by ticks. At 380 min, the vibration peaks due to the molecules in the second layer appear.

3.2. CuPc on Cu(110)

Figure 4(a) shows typical STM images of CuPc molecules on Cu(110) at the initial stage of adsorption. In contrast to the case of the adsorption on Cu(100), a dimer structure was predominantly observed on the terrace, with relatively few monomers (∼80% of CuPc adsorbs as dimer). Two equivalent orientations were observed for the dimer [Fig. 4(b)]. In the dimer, two of the four lobes of each molecule were brighter than the other two. This is ascribed to the surface reconstruction below the molecules. By displacing the molecules (Fig. S4), we found that "added row" was locally formed at the interface, as illustrated in Fig. 4(c). It is noted that the molecules adsorb preferentially at step sites and form chain-like structure along $[1\bar{1}0]$ (Fig. S5). Therefore, we postulate that the dimer with Cu row at the interface (dimer complex) is initially produced at the step, and then migrates across the surface at 300 K until it is stabilized in the form shown in Fig. 4(a). The adsorption in this dimeric configuration may increase the enthalpy gain of the system. As the coverage increases, larger clusters such as tetramer shown in Figs. 4(i) and 4(j) were observed on the terrace. This could be a precursor to the extended chain structure observed at higher coverage [35].

The monomers also exist on the surface at the initial coverage [Fig. 4(a)]. Their surface adsorption is intact and without surface reconstruction, as shown in Fig. S4. The molecule appears to be asymmetric with one of the lobes laterally protruding, as indicated by arrows in Figs. 4(d)-4(h), and were observed to exist in four equivalent orientations [Figs. 4(e)-4(h)]. Therefore the molecule adsorbs in a low-symmetry (C_1) configuration. The center Cu ion may prefer to bond to the three-coordinate site of the (111) microfacets. Although the monomer is a minority species on the surface, we focused on it to investigate the electronic states of CuPc on the intact Cu(110) surface. The STS recorded over each lobe of the monomer show two peaks at -0.13 and -0.05 V, with the intensities depending on the positions (Fig. 5). The former peak is relatively high in intensity for the spectra 1 and 3; in contrast, the latter peak is high for spectra 2 and 4. These peaks are ascribed to the split LUMO; because the symmetry is degraded upon adsorption, the degeneracy of LUMO is lifted and the peaks mainly appear at different positions between the two orthogonal molecular axes. Thus, the LUMO is located below E_{F} and is almost occupied. It is noted that the Fano effect (asymmetry in the peak), as observed for CuPc on Cu(100) [Fig. 2(a)], was not clearly detected in this case. Because the LUMO lies apart from E_{F} and the tunneling involves inelastic process, the interference between the

conductance channels might be hindered.

4. Discussion

Based on the STS measurements indicating partial and full occupation of LUMO, it can be concluded that the CuPc molecule is chemisorbed on Cu(100) and Cu(110), respectively. The chemical interaction of CuPc with Cu(100) is also inferred from the vibration spectra. The 77 meV peak is assigned to the OPB mode of the pyrrole ring and arises from the interaction with the surface, which was absent for CuPc physisorbed on Au(100) [51]. This new mode implies chemical bonding between the molecule and the surface.

When π-conjugated organic molecules are adsorbed on metal surfaces, charge transfer into the ligand π orbital (LUMO) and partial occupation may cause spin polarization of the molecule [37, 52, 53, 54, 55]. The spin polarization appears when the intramolecular Coulomb repulsion U is larger than the resonance width Γ of LUMO. This is the case of CuPc on Ag(100), where spin-split LUMO was observed below and above $E_{\rm F}$ with U=0.65 eV, and a sharp Kondo resonance peak with a width of $\sim$5 meV was observed at $E_{\rm F}$ at 4.8 K [37]. The Kondo resonance appears as a result of the screening of the spin moment of the molecule by itinerant metal electrons at low temperature [56]. For strongly interacting Cu–organic interfaces, the Kondo resonance due to ligand spin was observed with the width ranging from $\sim$10 meV for tetracyanoethylene on Cu(111) at 5.3 K [52] to $\sim$30 meV for titanyl phthalocyanine on Cu(110) at 5 K [55]. Likewise, the STS peak observed in Fig. 2(a) might be ascribed to the Kondo resonance as a result of electron transfer into LUMO of CuPc. However, the width of 0.2 eV observed for CuPc on Cu(100) is much larger than those for the Kondo resonance. Thus we propose that the strong hybridization causes the intramolecular Coulomb repulsion to almost disappear ($U \approx$0) and that the STS peak is ascribed to LUMO itself.

It is found that the LUMO of CuPc is positioned at $E_{\rm F}$ on Cu(100), and 0.13 and 0.05 eV below $E_{\rm F}$ on Cu(110). It was previously reported for Cu(111) that the LUMO is positioned at 0.6 eV below $E_{\rm F}$ by STS [26] and 0.4 eV below $E_{\rm F}$ by photoelectron spectroscopy [29]. Thus, the LUMO of CuPc decreases in energy in the order of Cu(100), Cu(110), and Cu(111). This is not in line with ϕ_0 (the work function of bare metal surface), which decreases in sequence as Cu(111), Cu(100), and Cu(110) [10, 57]. On strongly

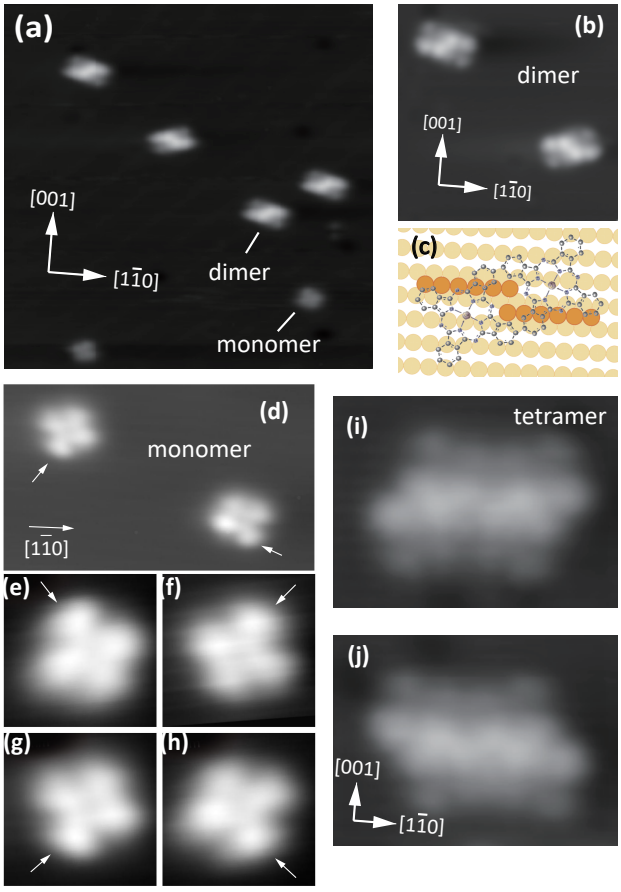

Figure 4: (a) Typical STM images of CuPc on Cu(110) at 6 K. The image size is 30 × 30 nm. The molecules are predominantly dimers on the surface, with relatively few monomers. (b) STM images of CuPc dimers (12 × 12 nm). (c) Schematic structure of the dimer. The kinked row of added Cu atoms is shown in deep orange. (d) STM images of CuPc monomers on Cu(110) (9.0 × 7.9 nm). The molecule is in the C_1 configuration with one of the lobes laterally protruding as indicated by the arrows. (e)–(h) The equivalent four orientations of CuPc on Cu(110). (i), (j) STM images of two equivalent forms of CuPc tetramer in different orientations (7.2×5.3 nm). All STM images were recorded at V_s=-0.4 V and I = 1 nA.

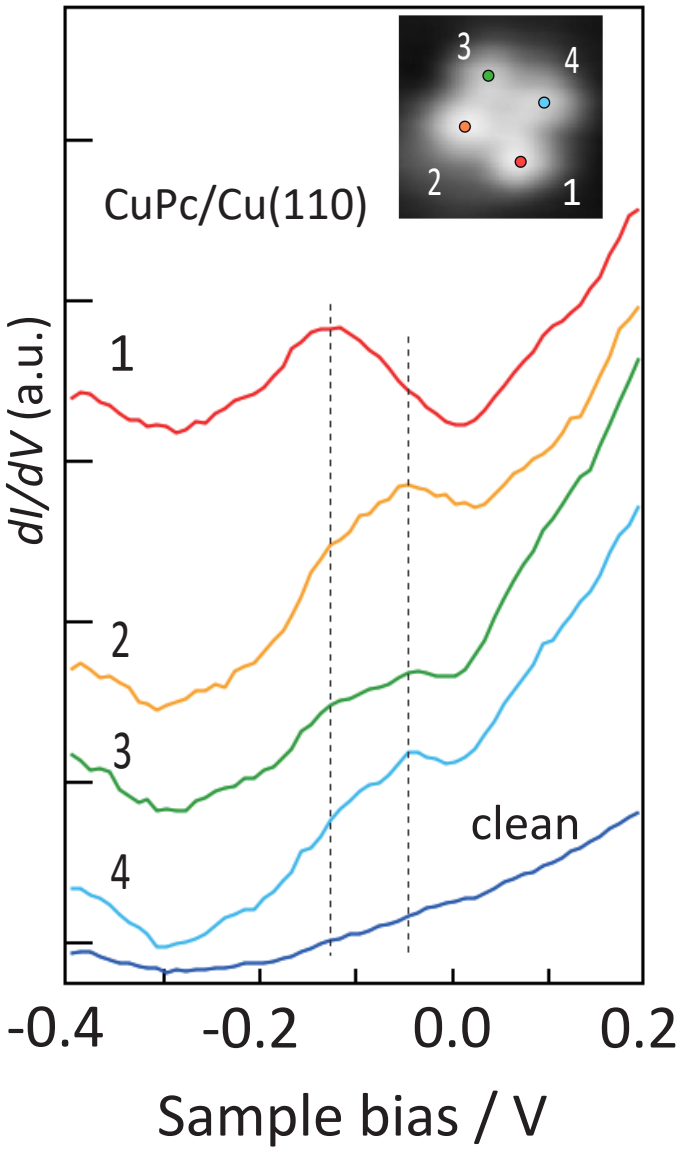

Figure 5: STS obtained for a CuPc monomer on Cu(110) at 6 K at each of the points indicated by the numbers in the inset. The bottom shows the spectrum recorded over the clean surface. The protruded lobe is indexed as number 1.

interacting Cu surfaces, the hybridization may play a major role in the energy level alignment. Intuitively, when the LUMO level is hybridized with Cu d band, it is repelled upward, depending on the coupling strength which is closely related to the electronic structure at the interface. Because the d-band center is located at higher energy for open surface, the interaction of LUMO with d band is larger and thus it is pushed to higher level. This might be the origin of the higher LUMO level of CuPc on Cu(100) and Cu(110) than that on Cu(111). Thus, the position of LUMO is determined by the hybridization with surface d band as well as by the electrostatic effect such as work function. The position of the d-band center has been argued to play an essential role in determining the reactivity of small molecules in heterogeneous catalysis [58, 59], which might also be an important factor for the energy level alignment of organic molecules.

5. Conclusions

CuPc adsorbs on Cu(100) with the center Cu ion located over the hollow site while maintaining a fourfold symmetry. The degenerate LUMO is positioned at E_{F} and is hence partially occupied. By contrast, CuPc adsorbs on Cu(110) with its molecular symmetry degraded to C_1. Consequently, the degeneracy is lifted, and the LUMO is split and positioned at 0.13 and 0.05 eV below E_{F}. It is proposed that the position of surface d-band center is an important factor for the energy level alignment and its structure dependence for these strongly coupled systems.

Declaration of Competing Interest

The authors declare that they have no known competing financial interests or personal relationships that could have appeared to influence the work reported in this paper.

Acknowledgement

We sincerely thank E. Minamitani, Y. Hamamoto, I. Hamada, Y. Morikawa for fruitful discussions. This work was supported by JSPS KAKENHI Grant Number 21H01886, 21K18202, and JST CREST Grant Number JPMJCR20R4, Japan.

Supplementary information

STM images of CuPc coadsorbed with oxygen atoms on Cu(100) (Fig. S1), STS for ZnPc/Cu(100) (Fig. S2), fitting of the STS curves of CuPc/Cu(100) to Fano formula (Fig. S3), STM image of added row below a CuPc dimer on Cu(110) and monomers (Fig. S4), and large-scale STM images of CuPc/Cu(110) (Fig. S5).

Appendix

With p-orbital tip, the STM image reflects the absolute square of the lateral gradient of the LUMO orbital as [43, 44]:

$$A_p(x, y, z_0) = |\frac{\partial\phi(x, y, z_0)}{\partial x}|^2 + |\frac{\partial\phi(x, y, z_0)}{\partial y}|^2 \quad (1)$$

where $\phi(x, y, z_0)$ represents the wavefunction of LUMO at a distance z_0 from the molecular plane. With normal s-orbital tip, the image reflects simply the absolute square of LUMO as:

$$A_s(x, y, z_0) = |\phi(x, y, z_0)|^2 \quad (2)$$

Because the LUMO is degenerate, the image represents the superposition of the absolute squares for the two orthogonal orbitals. The STM image of CuPc on Cu(100) recorded with NO-modified tip [Fig. 1(b)] is qualitatively consistent with $A_p(x, y, z_0)$ rather than $A_s(x, y, z_0)$. Figure A1 shows the comparison of the experimental image [Fig. A1(a)] with $A_p(x, y, z_0)$ [Fig. A1(b)] and $A_s(x, y, z_0)$ [Fig. A1(c)] for an isoindole moiety of CuPc. Specifically, the $A_p(x, y, z_0)$ shows finite tunneling amplitude along the isoindole (dashed lines) whereas the $A_s(x, y, z_0)$ shows no amplitude due to the nodal plane of the molecular orbital. In the same way, the surface Cu atoms (s character) appear to be depressed with a NO-modified tip [Fig. 1(b)].

References

[1] L. Zou, V. Savvate'ev, J. Booher, C.-H. Kim, J. Shinar, Combinatorial fabrication and studies of intense efficient ultraviolet–violet organic light-emitting device arrays, Appl. Phys. Lett. 79 (14) (2001) 2282–2284, doi.org/10.1063/1.1399004.

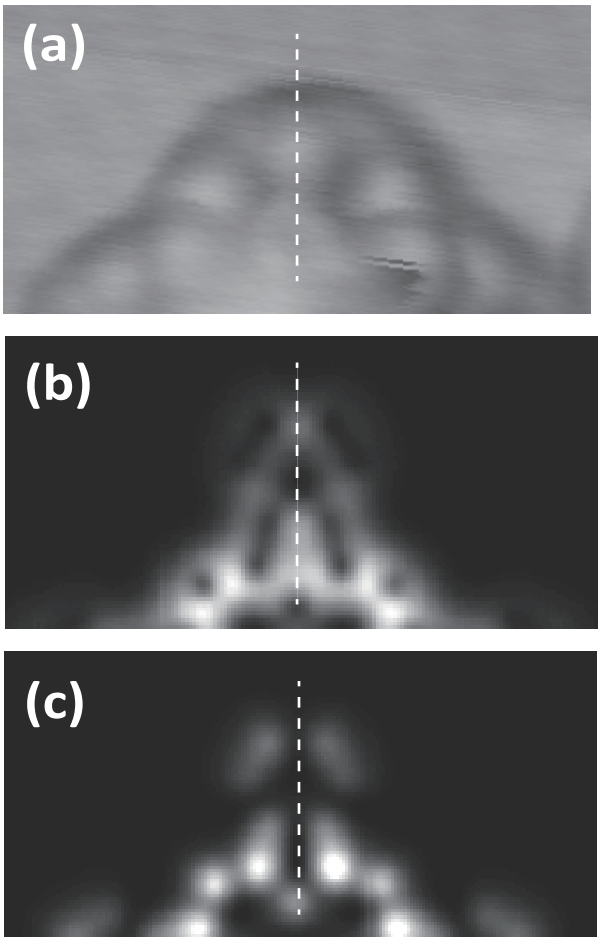

Figure 6: (a) Enlarged STM image for the isoindole of CuPc on Cu(100) obtained with a NO-modified tip [Fig. 1(b)]. (b) The corresponding images of $A_p(x, y, z_0)$ and (c) $A_s(x, y, z_0)$. The dashed lines represent the mirror plane along the isoindole group.

[2] F. Evers, R. Korytár, S. Tewari, J. M. van Ruitenbeek, Advances and challenges in single-molecule electron transport, Rev. Mod. Phys. 92 (2020) 035001, doi.org/10.1103/RevModPhys.92.035001.

[3] H. Ishii, K. Sugiyama, E. Ito, K. Seki, Energy level alignment and interfacial electronic structures at organic/metal and organic/organic interfaces, Adv. Mater. 11 (8) (1999) 605–625, doi.org/10.1002/(SICI)1521-4095(199906)11:8¡605::AID-ADMA605¿3.0.CO;2-Q.

[4] D. Cahen, A. Kahn, Electron energetics at surfaces and interfaces: Concepts and experiments, Adv. Mater. 15 (4) (2003) 271–277, doi.org/10.1002/adma.200390065.

[5] S. Braun, W. R. Salaneck, M. Fahlman, Energy-level alignment at organic/metal and organic/organic interfaces, Adv. Mater. 21 (14-15) (2009) 1450–1472, doi.org/10.1002/adma.200802893.

[6] M. Fahlman, S. Fabiano, V. Gueskine, D. Simon, M. Berggren, X. Crispin, Interfaces in organic electronics, Nature Reviews Materials 4 (10) (2019) 627–650. doi:10.1038/s41578-019-0127-y.

[7] J. W. Gadzuk, Surface molecules and chemisorption: I. adatom density of states, Surf. Sci. 43 (1) (1974) 44–60, doi.org/10.1016/0039-6028(74)90218-0.

[8] J. Muscat, D. Newns, Chemisorption on metals, Prog. Surf. Sci. 9 (1) (1978) 1 – 43, doi.org/10.1016/0079-6816(78)90005-9.

[9] J. K. Nørskov, Chemisorption on metal surfaces, Rep. Prog. Phys. 53 (10) (1990) 1253, doi.org/10.1088/0034-4885/53/10/001.

[10] M. Willenbockel, D. Lüftner, B. Stadtmüller, G. Koller, C. Kumpf, S. Soubatch, P. Puschnig, M. G. Ramsey, F. S. Tautz, The interplay between interface structure, energy level alignment and chemical bonding strength at organic–metal interfaces, Phys. Chem. Chem. Phys. 17 (2015) 1530–1548, doi.org/10.1039/C4CP04595E.

[11] X. Crispin, V. Geskin, A. Crispin, J. Cornil, R. Lazzaroni, W. R. Salaneck, J.-L. Brédas, Characterization of the interface dipole at organic/ metal interfaces, Journal of the American Chemical Society 124 (27) (2002) 8131–8141. doi:10.1021/ja025673r.

[12] S. Duhm, A. Gerlach, I. Salzmann, B. Bröker, R. Johnson, F. Schreiber, N. Koch, Ptcda on au(111), ag(111) and cu(111): Correlation of interface charge transfer to bonding distance, Org. Electron. 9 (1) (2008) 111 – 118, doi.org/10.1016/j.orgel.2007.10.004.

[13] N. Koch, Energy levels at interfaces between metals and conjugated organic molecules, J. Phys.: Condens. Matter 20 (18) (2008) 184008, doi.org/10.1088/0953-8984/20/18/184008.

[14] K. Toyoda, I. Hamada, K. Lee, S. Yanagisawa, Y. Morikawa, Density functional theoretical study of pentacene/noble metal interfaces with van der waals corrections: Vacuum level shifts and electronic structures, J. Chem. Phys. 132 (13) (2010) 134703. doi:10.1063/1.3373389.

[15] R. Otero, A. V. de Parga, J. Gallego, Electronic, structural and chemical effects of charge-transfer at organic/inorganic interfaces, Surf. Sci. Rep. 72 (3) (2017) 105 – 145, doi.org/10.1016/j.surfrep.2017.03.001.

[16] F. Tautz, Structure and bonding of large aromatic molecules on noble metal surfaces: The example of ptcda, Prog. Surf. Sci. 82 (9) (2007) 479 – 520, doi.org/10.1016/j.progsurf.2007.09.001.

[17] M.-T. Chen, O. T. Hofmann, A. Gerlach, B. Bröker, C. Bürker, J. Niederhausen, T. Hosokai, J. Zegenhagen, A. Vollmer, R. Rieger, K. Müllen, F. Schreiber, I. Salzmann, N. Koch, E. Zojer, S. Duhm, Energy-level alignment at strongly coupled organic–metal interfaces, J. Phys.: Condens. Matter 31 (19) (2019) 194002, doi.org/10.1088/1361-648x/ab0171.

[18] F. Widdascheck, A. A. Hauke, G. Witte, A solvent-free solution: Vacuum-deposited organic monolayers modify work functions of noble metal electrodes, Advanced Functional Materials 29 (17) (2019) 1808385. doi:https://doi.org/10.1002/adfm.201808385.

[19] A. Franco-Cañellas, S. Duhm, A. Gerlach, F. Schreiber, Binding and electronic level alignment of π-conjugated systems on metals, Reports on Progress in Physics 83 (6) (2020) 066501. doi:10.1088/1361-6633/ab7a42.

[20] P. S. Bagus, V. Staemmler, C. Wöll, Exchangelike effects for closed-shell adsorbates: Interface dipole and work function, Phys. Rev. Lett. 89 (2002) 096104. doi:10.1103/PhysRevLett.89.096104.

[21] N. D. Lang, A. R. Williams, Theory of atomic chemisorption on simple metals, Phys. Rev. B 18 (2) (1978) 616. doi:10.1103/PhysRevB.18.616.

[22] J. Kröger, H. Jensen, R. Berndt, R. Rurali, N. Lorente, Molecular orbital shift of perylenetetracarboxylic-dianhydride on gold, Chem. Phys. Lett. 438 (4) (2007) 249–253, doi.org/10.1016/j.cplett.2007.03.001.

[23] B. Hammer, J. K. Norskov, Why gold is the noblest of all the metals, Nature 376 (6537) (1995) 238–240. doi:10.1038/376238a0.

[24] Y. Zou, L. Kilian, A. Schöll, T. Schmidt, R. Fink, E. Umbach, Chemical bonding of ptcda on ag surfaces and the formation of interface states, Surf. Sci. 600 (6) (2006) 1240–1251, doi.org/10.1016/j.susc.2005.12.050.

[25] A. Kraft, R. Temirov, S. K. M. Henze, S. Soubatch, M. Rohlfing, F. S. Tautz, Lateral adsorption geometry and site-specific electronic structure of a large organic chemisorbate on a metal surface, Phys. Rev. B 74 (2006) 041402, doi.org/10.1103/PhysRevB.74.041402.

[26] J. Schaffert, M. C. Cottin, A. Sonntag, H. Karacuban, C. A. Bobisch, N. Lorente, J.-P. Gauyacq, R. Möller, Imaging the dynamics of individually adsorbed molecules, Nat. Mater. 12 (3) (2013) 223–227, doi.org/10.1038/nmat3527.

[27] S. Fremy-Koch, A. Sadeghi, R. Pawlak, S. Kawai, A. Baratoff, S. Goedecker, E. Meyer, T. Glatzel, Controlled switching of a single cupc molecule on cu(111) at low temperature, Phys. Rev. B 100 (2019) 155427, doi.org/10.1103/PhysRevB.100.155427.

[28] D. G. de Oteyza, A. El-Sayed, J. M. Garcia-Lastra, E. Goiri, T. N. Krauss, A. Turak, E. Barrena, H. Dosch, J. Zegenhagen, A. Rubio, Y. Wakayama, J. E. Ortega, Copper-phthalocyanine based metal–organic interfaces: The effect of fluorination, the substrate, and its symmetry, J. Chem. Phys. 133 (21) (2010) 214703, doi.org/10.1063/1.3509394.

[29] B. Stadtmüller, I. Kröger, F. Reinert, C. Kumpf, Submonolayer growth of cupc on noble metal surfaces, Phys. Rev. B 83 (2011) 085416, doi.org/10.1103/PhysRevB.83.085416.

[30] S.-H. Chang, S. Kuck, J. Brede, L. Lichtenstein, G. Hoffmann, R. Wiesendanger, Symmetry reduction of metal phthalocyanines on metals, Phys. Rev. B 78 (2008) 233409, doi.org/10.1103/PhysRevB.78.233409.

[31] I. Kröger, B. Stadtmüller, C. Kleimann, P. Rajput, C. Kumpf, Normal-incidence x-ray standing-wave study of copper phthalocyanine submonolayers on cu(111) and au(111), Phys. Rev. B 83 (2011) 195414, doi.org/10.1103/PhysRevB.83.195414.

[32] P. H. Lippel, R. J. Wilson, M. D. Miller, C. Wöll, S. Chiang, High-resolution imaging of copper-phthalocyanine by scanning-tunneling microscopy, Phys. Rev. Lett. 62 (1989) 171–174, doi.org/10.1103/PhysRevLett.62.171.

[33] T. J. Schuerlein, N. R. Armstrong, Formation and characterization of epitaxial phthalocyanine and perylene monolayers and bilayers on cu(100): Low-energy electron diffraction and thermal desorption mass spectrometry studies, J. Vac. Sci. Technol. A 12 (4) (1994) 1992–1997, doi.org/10.1116/1.578995.

[34] D. Lüftner, S. Weiß, X. Yang, P. Hurdax, V. Feyer, A. Gottwald, G. Koller, S. Soubatch, P. Puschnig, M. G. Ramsey, F. S. Tautz, Understanding the photoemission distribution of strongly interacting two-dimensional overlayers, Phys. Rev. B 96 (2017) 125402. doi:10.1103/PhysRevB.96.125402.

[35] M. Abadía, R. González-Moreno, A. Sarasola, G. Otero-Irurueta, A. Verdini, L. Floreano, A. Garcia-Lekue, C. Rogero, Massive surface reshaping mediated by metal–organic complexes, J. Phys. Chem. C 118 (51) (2014) 29704–29712, doi.org/10.1021/jp505802h.

[36] X. Yang, L. Egger, J. Fuchsberger, M. Unzog, D. Lüftner, F. Hajek, P. Hurdax, M. Jugovac, G. Zamborlini, V. Feyer, G. Koller, P. Puschnig, F. S. Tautz, M. G. Ramsey, S. Soubatch, Coexisting charge states in a

unary organic monolayer film on a metal, The Journal of Physical Chemistry Letters 10 (21) (2019) 6438–6445. doi:10.1021/acs.jpclett.9b02231.

[37] A. Mugarza, R. Robles, C. Krull, R. Korytár, N. Lorente, P. Gambardella, Electronic and magnetic properties of molecule-metal interfaces: Transition-metal phthalocyanines adsorbed on ag(100), Phys. Rev. B 85 (2012) 155437, doi.org/10.1103/PhysRevB.85.155437.

[38] C. Uhlmann, I. Swart, J. Repp, Controlling the orbital sequence in individual cu-phthalocyanine molecules, Nano Lett. 13 (2) (2013) 777–780, doi.org/10.1021/nl304483h.

[39] H. Koshida, H. Okuyama, S. Hatta, T. Aruga, Y. Hamamoto, I. Hamada, Y. Morikawa, Identifying atomic-level correlation between geometric and electronic structure at a metal–organic interface, J. Phys. Chem. C 124 (32) (2020) 17696–17701, doi.org/10.1021/acs.jpcc.0c04678.

[40] C. Krull, R. Robles, A. Mugarza, P. Gambardella, Site- and orbital-dependent charge donation and spin manipulation in electron-doped metal phthalocyanines, Nat. Mater. 12 (4) (2013) 337–343, doi.org/10.1038/nmat3547.

[41] H. Okuyama, H. So, S. Hatta, T. Frederiksen, T. Aruga, Effect of adsorbates on single-molecule junction conductance, Surf. Sci. 678 (2018) 169–176, doi.org/10.1016/j.susc.2018.04.024.

[42] K. Kuroishi, M. R. Al Fauzan, T. N. Pham, Y. Wang, Y. Hamamoto, K. Inagaki, A. Shiotari, H. Okuyama, S. Hatta, T. Aruga, I. Hamada, Y. Morikawa, A flat-lying dimer as a key intermediate in no reduction on cu(100), Phys. Chem. Chem. Phys. 23 (2021) 16880–16887, doi.org/10.1039/D1CP02746H.

[43] L. Gross, N. Moll, F. Mohn, A. Curioni, G. Meyer, F. Hanke, M. Persson, High-resolution molecular orbital imaging using a p-wave stm tip, Phys. Rev. Lett. 107 (2011) 086101, doi.org/10.1103/PhysRevLett.107.086101.

[44] C. J. Chen, Tunneling matrix elements in three-dimensional space: The derivative rule and the sum rule, Phys. Rev. B 42 (1990) 8841–8857, doi.org/10.1103/PhysRevB.42.8841.

[45] L. Chen, Z. Hu, A. Zhao, B. Wang, Y. Luo, J. Yang, J. G. Hou, Mechanism for negative differential resistance in molecular electronic devices: Local orbital symmetry matching, Phys. Rev. Lett. 99 (2007) 146803. doi:10.1103/PhysRevLett.99.146803.

[46] M. Plihal, J. W. Gadzuk, Nonequilibrium theory of scanning tunneling spectroscopy via adsorbate resonances: Nonmagnetic and kondo impurities, Phys. Rev. B 63 (2001) 085404, doi.org/10.1103/PhysRevB.63.085404.

[47] A. E. Miroshnichenko, S. Flach, Y. S. Kivshar, Fano resonances in nanoscale structures, Rev. Mod. Phys. 82 (2010) 2257–2298, doi.org/10.1103/RevModPhys.82.2257.

[48] T. Kobayashi, F. Kurokawa, N. Uyeda, E. Suito, The metal-ligand vibrations in the infrared spectra of various metal phthalocyanines, Spectrochim. Acta Part A: Mol. Spectrosc. 26 (6) (1970) 1305–1311, doi.org/10.1016/0584-8539(70)80036-8.

[49] S. Hayashi, M. Samejima, Surface-enhanced raman scattering from copper phthalocyanine thin films, Surface Science 137 (2) (1984) 442–462, doi.org/10.1016/0039-6028(84)90522-3.

[50] Z. Liu, X. Zhang, Y. Zhang, J. Jiang, Theoretical investigation of the molecular, electronic structures and vibrational spectra of a series of first transition metal phthalocyanines, Spectrochim. Acta Part A: Mol. BioMol. Spectrosc. 67 (5) (2007) 1232–1246, doi.org/10.1016/j.saa.2006.10.013.

[51] J. Auerhammer, M. Knupfer, H. Peisert, J. Fink, The copper phthalocyanine/au(100) interface studied using high resolution electron energy-loss spectroscopy, Surf. Sci. 506 (3) (2002) 333–338, doi.org/10.1016/S0039-6028(02)01517-0.

[52] T. Choi, S. Bedwani, A. Rochefort, C.-Y. Chen, A. J. Epstein, J. A. Gupta, A single molecule kondo switch: Multistability of tetracyanoethylene on cu(111), Nano Lett. 10 (10) (2010) 4175–4180, doi.org/10.1021/nl1024563.

[53] U. G. E. Perera, H. J. Kulik, V. Iancu, L. G. G. V. Dias da Silva, S. E. Ulloa, N. Marzari, S.-W. Hla, Spatially extended kondo state in

magnetic molecules induced by interfacial charge transfer, Phys. Rev. Lett. 105 (2010) 106601, doi.org/10.1103/PhysRevLett.105.106601.

[54] T. Komeda, H. Isshiki, J. Liu, Y.-F. Zhang, N. Lorente, K. Katoh, B. K. Breedlove, M. Yamashita, Observation and electric current control of a local spin in a single-molecule magnet, Nat. Commun. 2 (1) (2011) 217, doi.org/10.1038/ncomms1210.

[55] B. Maughan, P. Zahl, P. Sutter, O. L. A. Monti, Ensemble control of kondo screening in molecular adsorbates, J. Phys. Chem. Lett. 8 (8) (2017) 1837–1844, doi.org/10.1021/acs.jpclett.7b00278.

[56] T. Komeda, Spins of adsorbed molecules investigated by the detection of kondo resonance, Surface Science 630 (2014) 343–355. doi:https://doi.org/10.1016/j.susc.2014.07.012.

[57] J. Wang, S.-Q. Wang, Surface energy and work function of fcc and bcc crystals: Density functional study, Surf. Sci. 630 (2014) 216 – 224, doi.org/10.1016/j.susc.2014.08.017.

[58] B. Hammer, J. Nørskov, Electronic factors determining the reactivity of metal surfaces, Surface Science 343 (3) (1995) 211–220. doi:https://doi.org/10.1016/0039-6028(96)80007-0.

[59] J. K. Nørskov, T. Bligaard, B. Hvolbæk, F. Abild-Pedersen, I. Chorkendorff, C. H. Christensen, The nature of the active site in heterogeneous metal catalysis, Chem. Soc. Rev. 37 (2008) 2163–2171. doi:10.1039/B800260F.